A Survey of Rotor Loads Distribution In Maneuvering Flight

Robert M. Kufeld, Jeffrey L. Cross
Aerospace Engineers
NASA Ames Research Center
Moffett Field, California

William G. Bousman
Research Scientist
U.S. Army Aeroflightdynamics Directorate (ATCOM)
Moffett Field, California

Abstract

Maneuver data obtained under the NASA Ames/Army UH-60A Airloads Program are examined qualitatively to show the effects of maneuvering flight conditions on rotor load distributions. Specitic measurments obtained in pull-ups, roll reversals, and pushovers are examined and compared to level flight conditions. The effect of vortex interaction on blade and control loads and changes in lift distribution caused by pitch rate of the rotor during maneuvers is illustrated.

Notation

$\frac{C_{FM}}{\sigma} = \frac{M_F}{\pi\sigma\rho\Omega^2 R^5}$ flap bending

$\frac{C_{CM}}{\sigma} = \frac{M_E}{\pi\sigma\rho\Omega^2 R^5}$ chordwise bending

$\frac{C_{TM}}{\sigma} = \frac{M_T}{\pi\sigma\rho\Omega^2 R^5}$ torsional moment

$\frac{C_{PL}}{\sigma} = \frac{P}{\pi\sigma\rho\Omega^2 R^4}$ pitch link force

$\frac{C_Q}{\sigma} = \frac{Q_{MR}}{\pi\sigma\rho\Omega^2 R^5}$ main rotor shaft torque

$\frac{C_W}{\sigma} = \frac{GW}{\pi\sigma\rho\Omega^2 R^4}$ gross weight coefficient

$M^2 C_L = \frac{2L}{a^2 \rho c}$ normal force

$M^2 C_M = \frac{2C_m}{a^2 \rho c^2}$ section pitching moment coefficient

$M^2 C_{pu} = \frac{2(p - p_\infty)}{a^2 \rho c}$ upper sufface pressure coefficient

L	section lift, lbs
M	local Mach number
M_F	flap bending moment, in-lbs
M_E	edge bending moment, in-lbs
M_T	torsional moment, in-lbs
P	pitch-link force, lbs
Q_{MR}	main rotor shaft torque, ft-lbs
n_z	load factor, g
R	blade radius, ft
a	speed of sound, ft/sec
b	number of blades
c	blade chord, in
Ω	rotor speed, rad/sec
μ	advance ratio
ρ	air density, slug/ft^3
σ	rotor solidity
ψ	rotor azimuth, deg.

Presented at the American Helicopter Society Aeromechanics Specialists Conference, San Francisco, California, January 19-21, 1994.

Introduction

Structural loads will, for certain maneuvers, greatly exceed those encountered in level flight. In some cases maneuver-induced loads may determine the size of blade and control system components. Maneuver loads are not adequately predicted by theoretical methods and it is necessary in the development of new aircraft to rely on existing and appropriate flight test data to estimate maneuver loads.

A UH-60A Black Hawk, with a highly instrumented rotor, has been used in research flights at NASA-Ames Research Center since September 1993 and, as a part of this flight program, has obtained data for a number of different maneuvers. This paper examines a limited number of these maneuvers and, in a qualitative examination of the airloads on the blade, attempts to understand the sources of high structural loads in maneuvers.

Flight Test Data

Highly-instrumented blades have been designed, built, and installed on a standard UH-60A aircraft (Ref. 1). The first blade has a total of 221 pressure transducers installed in nine spanwise arrays as shown in Figure 1 plus an additional 21 pressure transducers installed near the leading edge between the spanwise arrays. The second blade is instrumented with strain gauges and accelerometers to measure the blade structural loads and response. The aircraft is also instrumented to measure the vehicle state and numerous other parameters (Ref. 1).

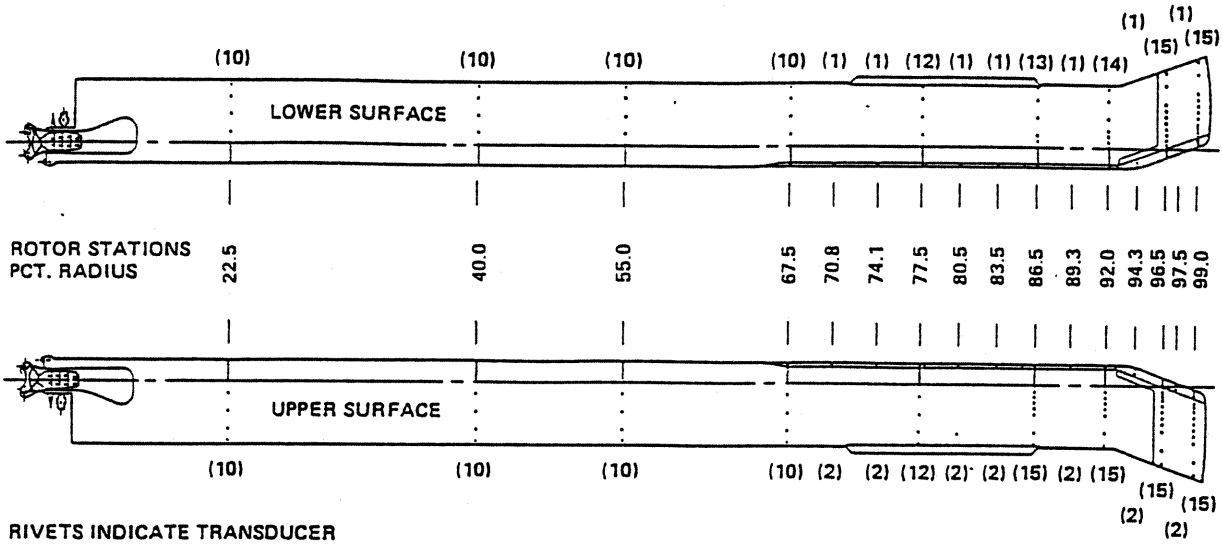

Fig. 1 UH-60A instrumented blade showing locations of the pressure transducers.

The data are sampled and digitized in the rotating system and a PCM stream is fed down though a slip ring at a data rate of approximately 7.5 Mbits/sec. The pressure data are sampled at 2142 Hz which corresponds to approximately 500 samples/revolution. However, anti-aliasing filters are set at about 500 Hz so that the effective sample rate is about 120 samples/revolution. Structural data are recorded at a lower rate which corresponds to about 24 samples/revolution.

A limited set of maneuvers have been flown during the program as shown in Table 1. Three maneuver conditions have been selected for discussion in this paper and are compared in Figure 2 with the rotor thrust coefficient boundary measured by McHugh (Ref. 2). For purposes of comparison the rotor weight coefficient/solidity has been multiplied by the measured load factor to define an effective rotor thrust coefficient/solidity.

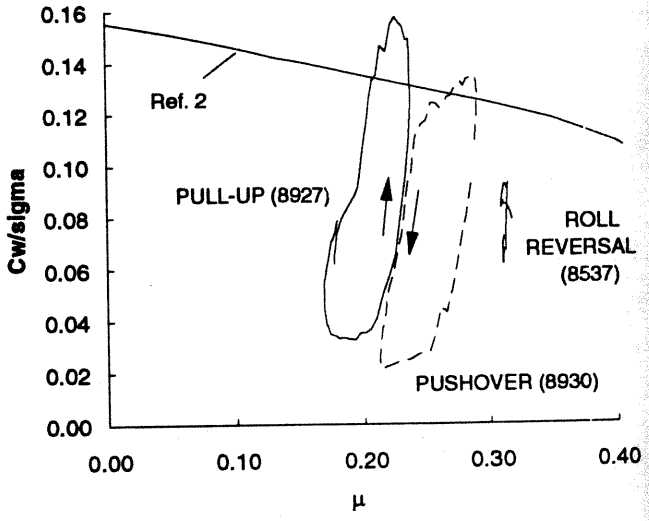

Fig. 2 Thrust as a function of advance ratio for selected maneuvers.

Maneuver	No. Test Points
Steady, Banked Turns	11
Symmetric Pull-ups	4
Symmetric Pushovers	2
Roll Reversals	5
Accelerations	1
Decelerations	2
Settling with Power	2

Table 1. - UH-60A Flight Test Maneuvers.

The first maneuver is a symmetric pushover with a target load factor of 0.25g at an indicated airspeed of 80 knots (KIAS). The maneuver is initiated by a dive, the aircraft is then pulled up so that the load factor exceeds 1g, and then the aircraft is pushed over so that the reduced load factor can be obtained. For this maneuver data were obtained at load factors both above and below 1g as shown in Figure 2. For a short portion of the maneuver, the equivalent C_W/σ exceeds the Ref. 2 boundary.

The second maneuver is a roll reversal with an entry speed of 120 KIAS and a target roll rate of 45 deg./sec. There is little change in load factor during this maneuver as indicated in Figure 2.

The third maneuver is a 2g pull-up. This maneuver is initiated with a pushover that includes reduced load factor and then the aircraft is rapidly pulled up and the peak load factor is obtained. In Figure 2 this pull-up appears similar to the pushover although the order of the maneuver is reversed. However, as discussed below, the pitch rates involved in this third maneuver are much higher and the resulting structural loads are also higher.

Maneuver Analysis

To some extent an aircraft in maneuvering flight can be said to be undergoing a steady maneuver or an unsteady maneuver. In the former case, if the angular rates are constant (and this implies that the control motions are stationary as well), then the maneuver can be considered steady. The best example of a steady maneuver is a constant-altitude, banked turn where the pitch rate and yaw rate are constant (and non-zero) while the roll rate is zero. Steady maneuvers are important in selecting data to test analyses as they represent a first step beyond a standard level flight condition where all angular rates are zero. (In this sense a steady flight condition is a degenerate steady maneuver or zeroth order maneuver.) It would be useful for the analyst to obtain steady maneuvers in single axes, that is, a constant pitch rate with zero roll and yaw rates and so forth. In practical cases, however, this can only be roughly approximated.

Unsteady maneuvers include angular accelerations as well as rates and are clearly more difficult for the analyst. Unsteady maneuvers also show additional complexity depending on whether the motion is largely occuring in one axis or more than one axis. For example, a symmetric pullout exhibits angular accelerations primarily in pitch while a rolling pullout has large angular accelerations in both the pitch and roll axes.

The air and structural loads measured on the UH-60A will be examined in a quasi-static manner. That is, each rotor revolution during the maneuver will be treated as a separate event and, for each event, the data point at an azimuth angle of 360 deg. will be assumed to be identical to the first sample point at zero degrees. Each rotor revolution or cycle is defined when Blade 1 (the pressure blade) passes over the tail of the aircraft. The rotor speed does vary during maneuvers and, therefore, the number of points obtained during one revolution also varies. However, an azimuth clock in combination with interpolation is used in the data reduction process to avoid difficulties with varying length records. Because this approach uses an azimuth clock; data obtained on blades other than Blade 1 will be offset in true time by the appropriate fraction of a revolution. None of the assumptions used in this quasi-static approach affect conclusions drawn from the analysis of the data.

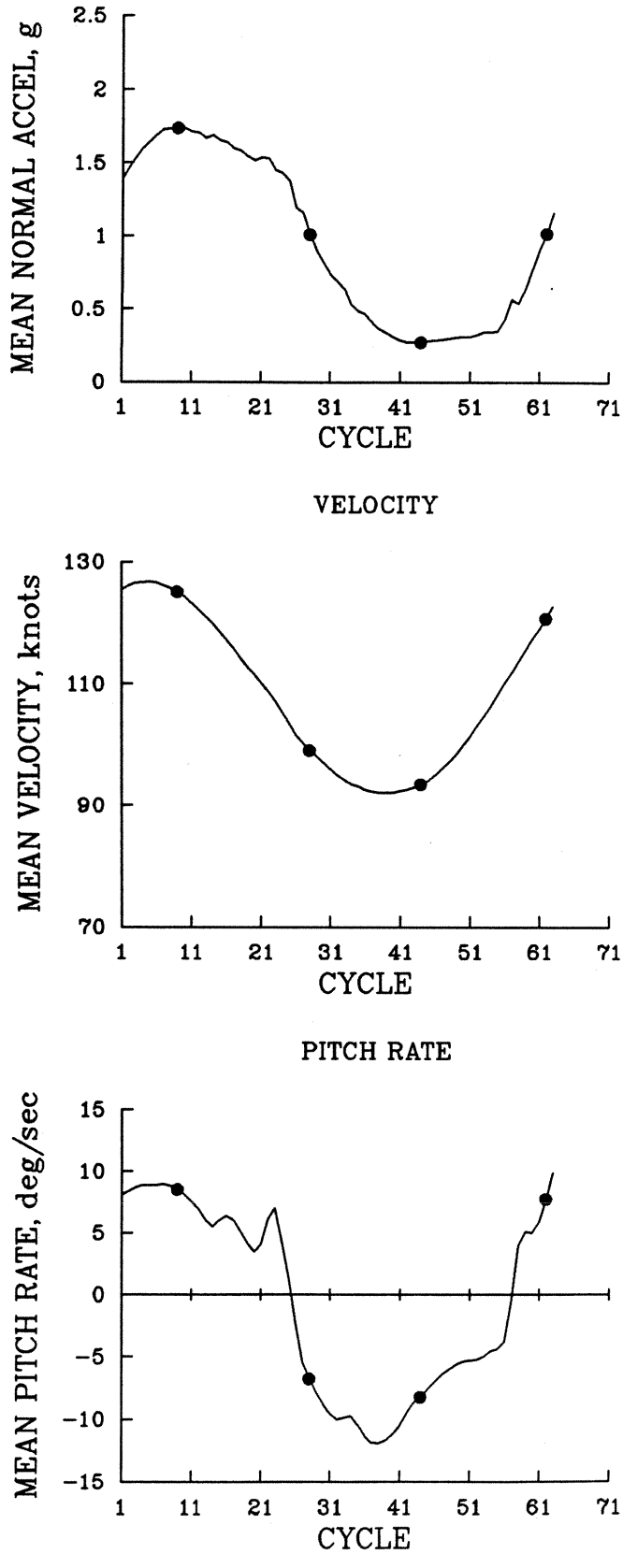

Fig. 3 Mean load factor, velocity, and pitch rate during pushover maneuver (8930).

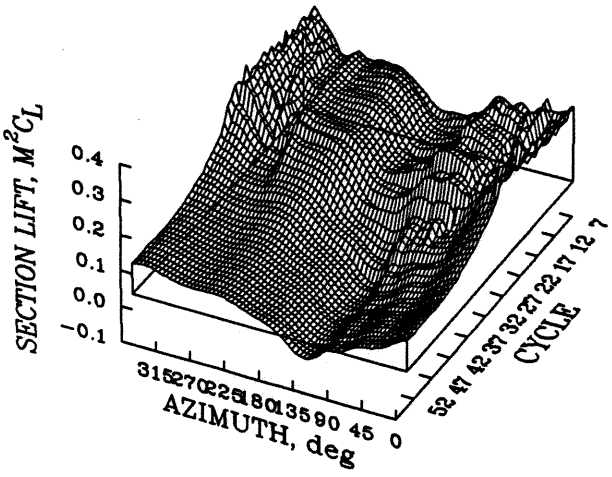

Fig. 4 Section lift at 0.865R as a function of azimuth and cycle count during pushover maneuver (8930); 0 to 60 harmonics.

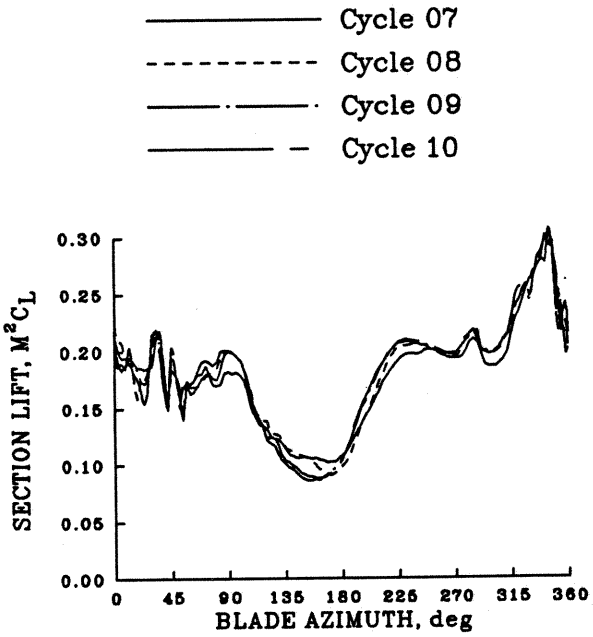

Fig. 5 Section lift at 0.865R during pushover maneuver (8930) for four adjacent revolutions; 0 to 60 harmonics

Pushover Maneuver

A pushover maneuver with a target of 0.25g at 80 KIAS recorded on Flight 89 as Counter 30 and 19 seconds of data were obtained during the maneuver. Three parameters that characterize the maneuver time history are shown in Figure 3 for the first 15 seconds of the record (63 cycles or revolutions). At the start of the data record the aircraft is in a slight dive and is pulling about 1.4g. The pitching rate is positive and the load factor increases to a peak of 1.7g from cycles 7 to 10. Cycle 9, in the middle of this range is marked with a solid circle and will be one of the cycles examined in detail. Following the load factor peak airspeed decreases slowly and near Cycle 21 the controls are moved to achieve the reduced load factor. At Cycle 28 (solid circle) the aircraft goes through 1g and by Cycle 44 (solid circle) reaches a load factor of 0.27g, close to the target value. The aircraft nose is dropping and recovery is initiated around Cycle 54 and the aircraft passes through 1g again at Cycle 62 (solid circle).

The section lift at 0.865R is shown in Figure 4 during the maneuver for cycles 7 to 54 as a function of blade azimuth and cycle count. The development of the section lift is seen as one moves from the rear of this surface plot to the front. Section lift is quite high, as expected, at the beginning of the maneuver and is rapidly reduced as the load factor approaches 0.25g.

From cycles 7 to 10 the load factor varies no more than 0.004g from a mean value of 1.733g. Figure 5 shows the section lift at 0.865R for these four cycles and it is seen that there is very little variation from cycle to cycle. Over this same period the advance ratio is decreasing from 0.291 to 0.287 and the pitch rate is dropping from 8.94 deg/sec to 8.14 deg/sec. This maneuver, over these four cycles, approximates a steady maneuver.

Figure 6 compares the measured distribution of section lift for Cycle 9 with measurements from a steady flight condition with $C_W/\sigma = 0.134$ (Flight 90, Counter 17). The product, $n_z(C_W/\sigma)$, for Cycle 9 is also 0.134 and, therefore, these conditions are roughly comparable. The distribution of lift for these two cases is noticeably different. The level flight case shows a strong reduction in lift in the second quadrant of the disk, particularly near the blade tip, that is required for roll moment balance. In the fourth quadrant the lift oscillates as the blade undergoes two cycles of dynamic stall. Under the maneuver conditions of Cycle 9 the lift is observed to occur more inboard than for level flight and the reduction in lift near the blade tip is broadened and moves more to the front of the disk. No stall cycles are apparent in the fourth quadrant, but it appears that vortex loading in the first quadrant is increased substantially.

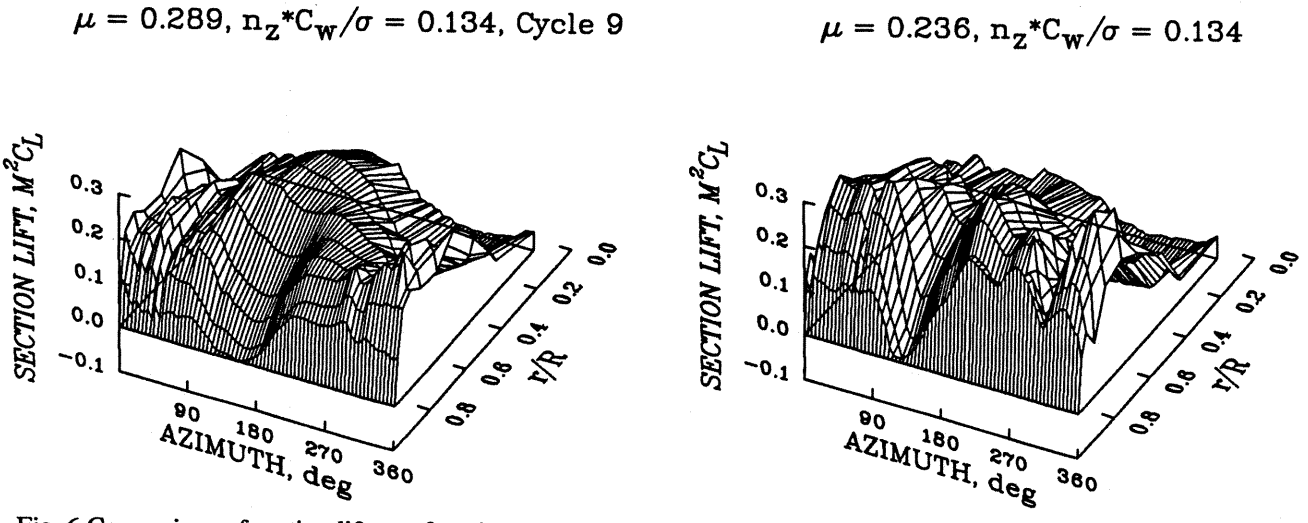

Fig. 6 Comparison of section lift as a function of azimuth and radial station for Cycle 9 of the pushover maneuver (8930) and an equivalent level flight case (9017); 0 to 60 harmonics.

The comparison of Cycle 9 with level flight data is extended in Figure 7 where the section lift and moment at 0.775R is compared to the $C_w/\sigma = 0.134$ case as before and also to level flight at moderate thrust, $C_w/\sigma = 0.079$ (Flight 85, Counter 27). The section lift for the maneuver condition at this radial station shows increased lift relative to the $C_w/\sigma = 0.079$ level case, but less that for the $C_w/\sigma = 0.134$ level case. The largest qualitative difference seen are the absence of dynamic stall in the third and fourth quadrants for the maneuver condition and the increased vortical wake loading in the first quadrant.

Some flavor of the complexity of the airloads during the high load factor portion of the maneuver is shown in Figure 8 where the upper surface pressures measured at six chord stations are shown at 0.865R. The heavy dashed line added to this figure represents the critical C_p boundary in the M^2C_{pu} format used here. In the first quadrant a number of mild blade vortex interactions are noted along the chord. Over the front of the airfoil the flow appears mildly supercritical, but no strong shock motions are exhibited until a chord of 0.203c is reached. At the end of the third quadrant and in the fourth quadrant three to four strong blade vortex interactions are seen and it appears that the one at ψ = 315 deg. is partly responsible for instituting a small stall pocket. This stall pocket extends to the trailing edge at about 355 degrees, but is of very short duration.

In terms of structural loading of the blade the pushover maneuver being examined here is relatively benign, particularly in flap and chord bending moments. The pitch-link loads are increased during the high load factor portion of the maneuver and Figure 9 compares the Blade 1 pitch-link loads with the two steady flight cases discussed previously. The oscillatory pitch-link loads for

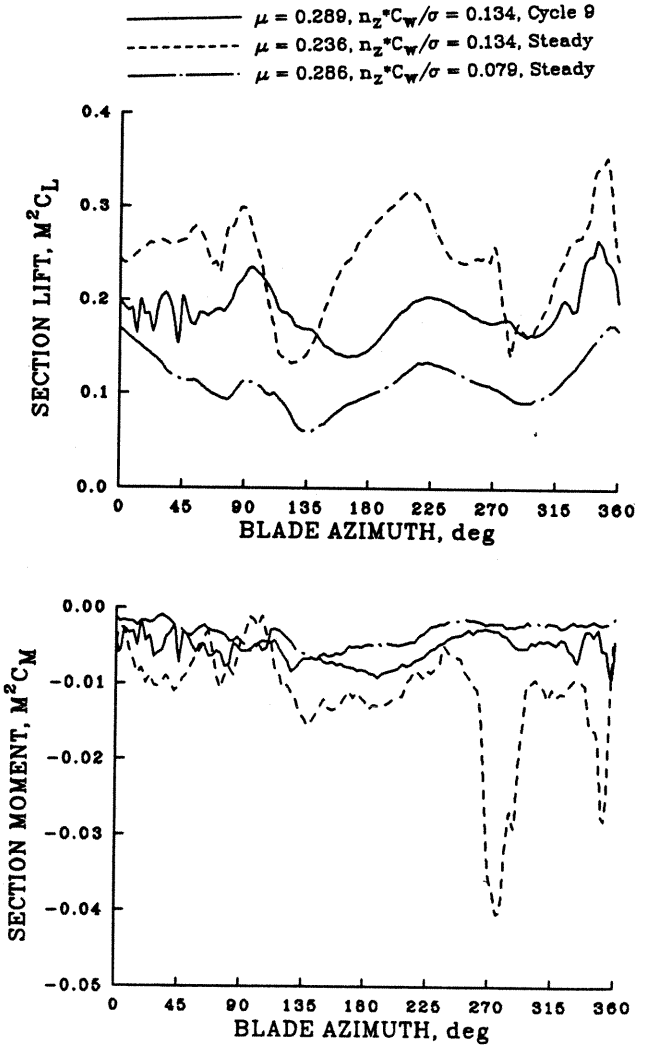

Fig. 7 Comparison of section lift and moment at 0.775R for Cycle 9 of the pushover maneuver (8930) and two level flight flight condition; 0 to 60 harmonics.

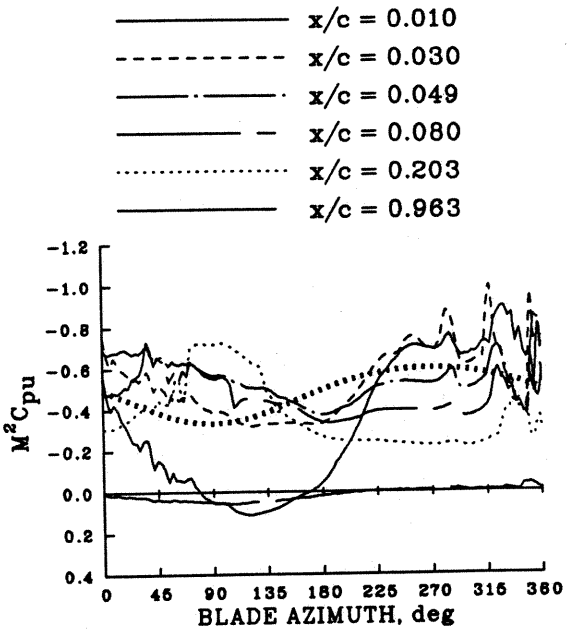

Fig. 8 Upper surface pressure at 0.865R for six chord locations for Cycle 7 of the pushover maneuver (8930); 0 to 60 harmonics.

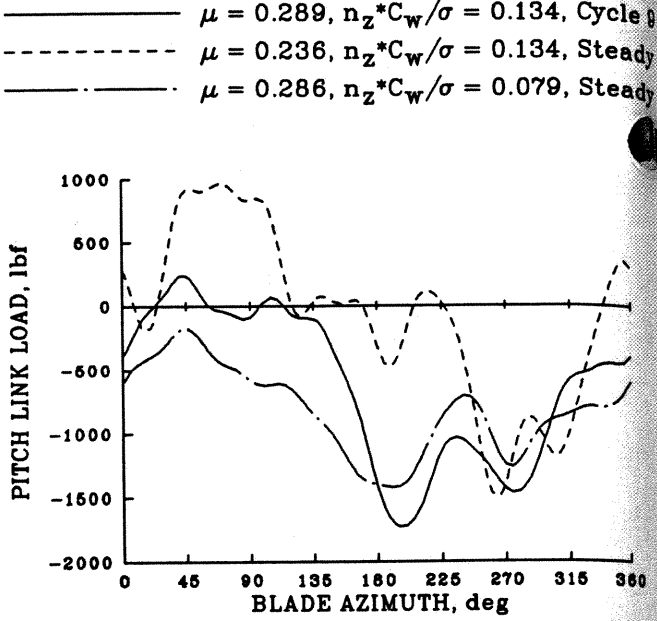

Fig.9 Comparison of pitch-link loads for Cycle 9 of the pushover maneuver(8930) and two level flight conditions; 0 to 12 harmonics

$\mu = 0.233$, $n_z*C_w/\sigma = 0.082$, Cycle 28

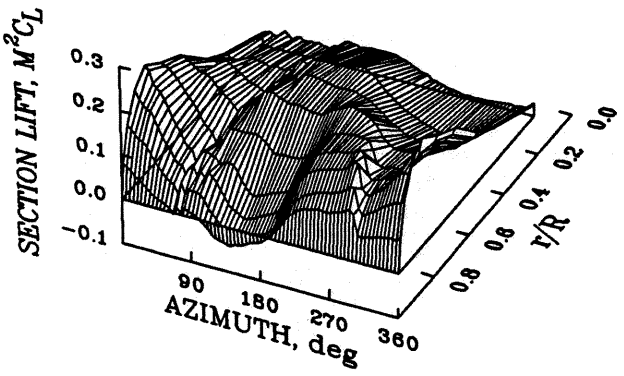

$\mu = 0.282$, $n_z*C_w/\sigma = 0.081$, Cycle 62

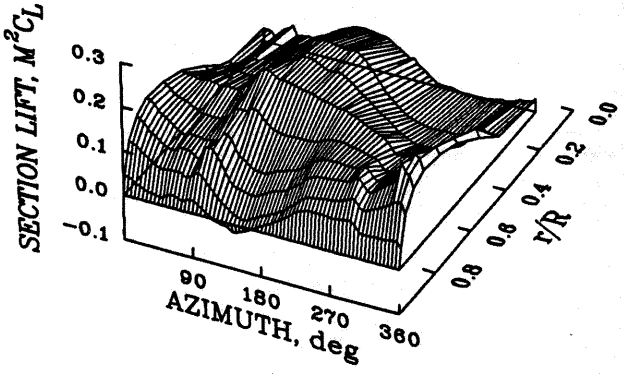

$\mu = 0.215$, $n_z*C_w/\sigma = 0.012$, Cycle 44

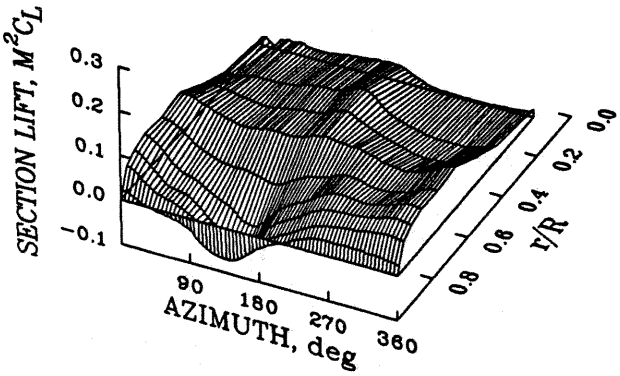

$\mu = 0.232$, $n_z*C_w/\sigma = 0.079$

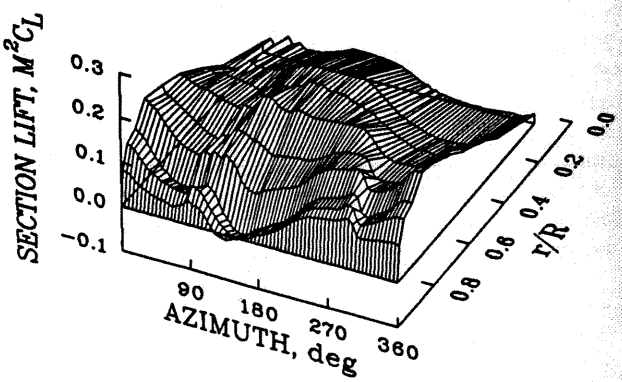

Fig. 10 Comparison of section lift as a function of azimuth and radial station for cycle 28, 44, and 62 of the pushover maneuver (8930) and an equivalent level flight case (8525); 0 to 60 harmonics.

Cycle 9 are increased by about 60% in comparison to those obtained in level flight at a moderate thrust coefficient. More interesting, however, is that the pitch-link load behavior is similar to the level flight case and shows no evidence of dynamic stall as is seen for the $C_W/\sigma = 0.134$ case. The primary source of the loading in level flight is an advancing side phenomena related to unsteady pitching motion of the blade and three-dimensional effects (Ref. 3) and it appears that this same source of loads governs for this maneuver case. In this sense the level flight loading is an approximate analog to the maneuver condition.

The section lift for three other cycles in the pushover maneuver are compared to a level flight case, $C_W/\sigma = 0.079$ (Flight 85, Counter 25), in Figure 10. Cycles 28 and 62 are for a load factor of 1g and the product $n_z(C_W/\sigma)$ for both cycles are quite close to the level flight case shown. The pitch rate, of course, is quite different being -6.7 deg/sec for Cycle 28 and +7.7 deg/sec for Cycle 62. In addition, the section lift distribution for the minimum load factor point (Cycle 44) is included in this figure as well. The three $n_z(C_W/\sigma) = 0.08$ cases are qualitatively very similar. All show the reduced lift in the second quadrant near the blade tip that is forced by roll moment balance (not so extreme at this moderate advance ratio) and the effects of the vortex loading on the advancing side and on the retreating side. Small differences are observed: Cycle 28 appears to show more discrete vortical effects on the advancing side while Cycle 62 shows slightly more lift inboard on the blade over the nose of the aircraft. However, the lift distributions are quite similar and the level flight case tends to split the differences when the lift for the two maneuver cycles is compared. The Cycle 44 lift is much reduced and this is expected as the blade is very lightly loaded for this reduced load factor condition.

Roll Reversal

A roll reversal maneuver with a target of 45 degrees per second roll rate was recorded on Flight 85 as Counter 37 and 15 seconds of data were obtained. The maneuver was initiated at 120 KIAS with a roll attitude of 38 degree right wing down. A rapid lateral stick deflection of 40% achieved a maximum roll rate of -45 degree per second (to the left). Airspeed bleed off and pitch attitude changes were minimized as much as possible. Figure 11 shows rotor cycle base time history of both roll attitude and roll rate during the maneuver. The maximum roll rate was held for about two rotor revolutions. Figure 11 also shows the effect of this maneuver on oscillatory (half peak-to-peak) pitch link load. It is easily seen that the maneuver more that doubles the loads on the push rod. For the purpose of this paper two cycles have been selected for comparison to level flight, cycle 26 and 30 (solid circles).

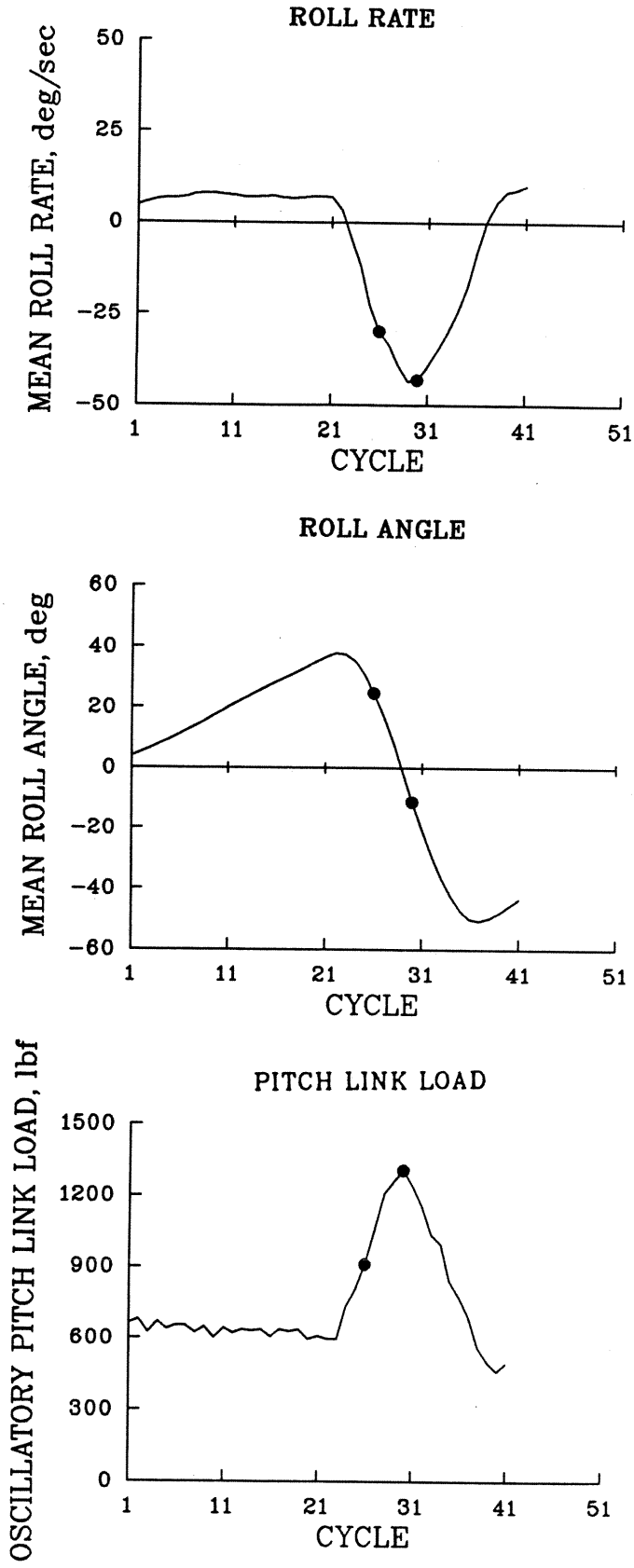

Fig. 11 Mean roll rate, roll angle and oscillatory pitch link load during roll reversal maneuver (8537).

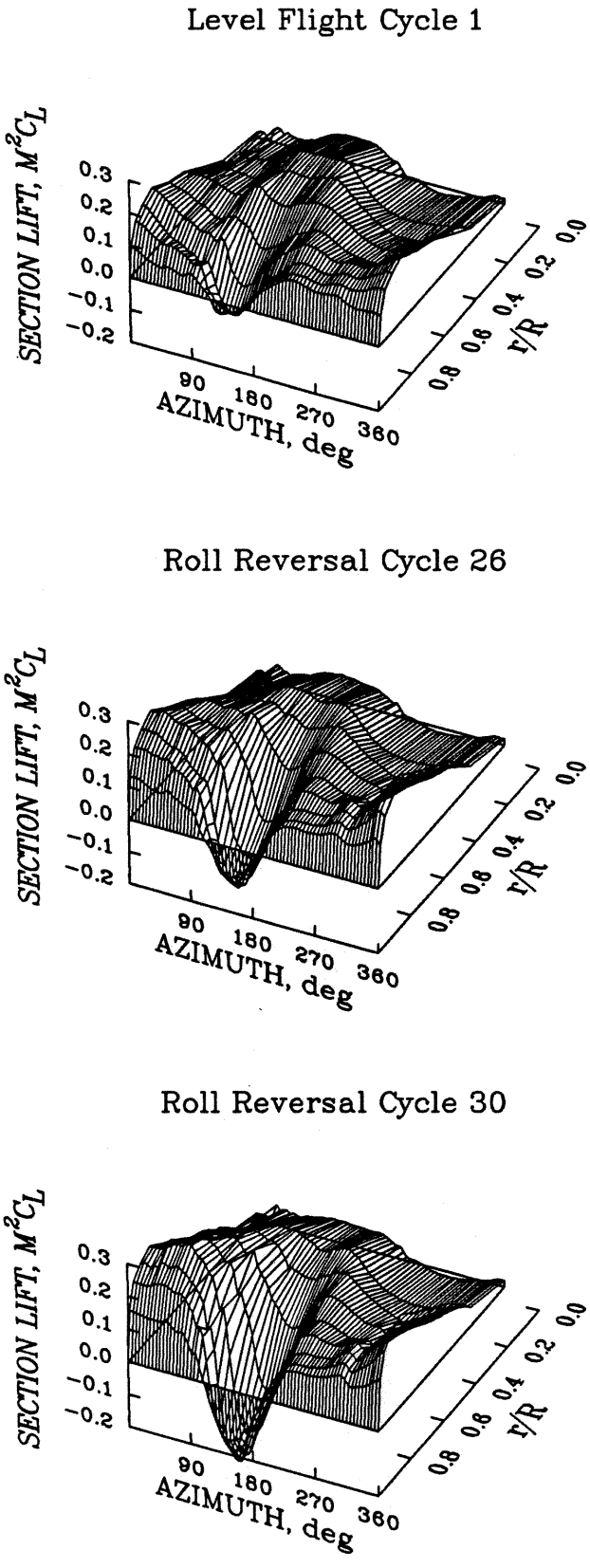

Fig 12 Comparison of section lift as a function of azimuth and radial station for cycle 26 and 30 of the roll reversal maneuver (8537) and an equivalent level flight case (8529); 0 to 60 harmonics.

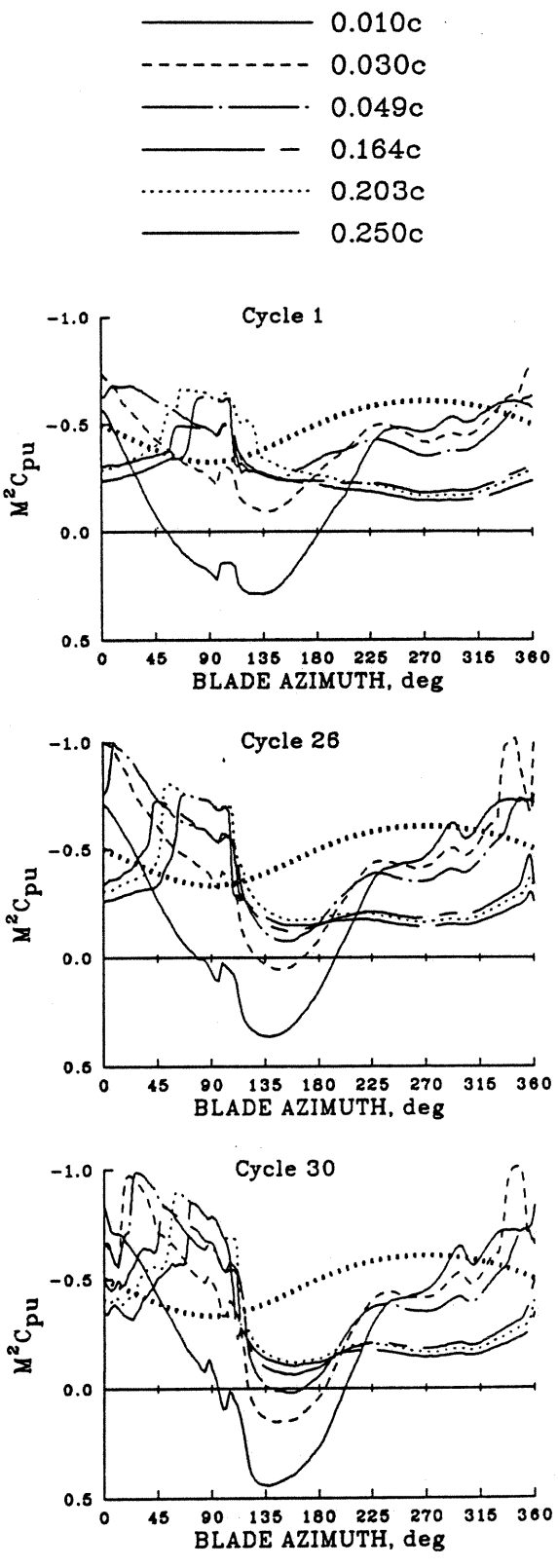

Fig. 13 Comparison of upper surface pressure at 0.865R for six chord locations for cycle 26 and 30 of the roll reversal maneuver (8537) and an equivalent level flight case (8529); 0 to 60 harmonics.

Figure 12 compares the measured section lift forces as a function of azimuth and radial station for one cycle of level flight at comparable airspeed and C_W/σ (Flight 85, Counter 29) to the two roll reversal cycles identified above. The level flight forces show the typical loading distribution of an articulated rotor with negative load at the tip in the second quadrant for roll moment balance and slight effect of blade vortex interaction on both the advancing and retreating sides of the rotor. As the roll rate increases the loading in the first quadrant increases greatly to nearly three times the value of level flight. The negative loading in the second quadrant also increases substantially. The loads closely match level flight on the retreating side of the disk. Evidence of blade vortex interaction is also visible on the advancing and retreating sides.

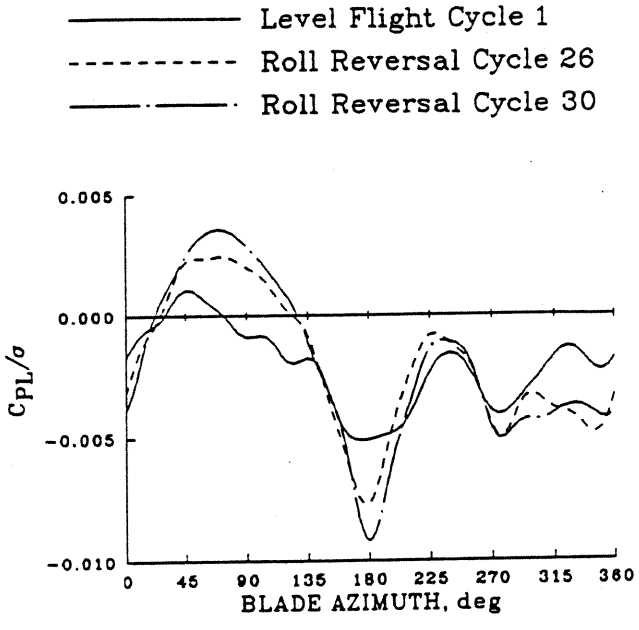

Fig. 14 Comparsison of pitch link load for cycle 26 and 30 of the roll reversal maneuver (8537) and an equivalent level flight case (8529); 0 to 12 harmonics.

A detailed look at the upper surface pressure for the three cycles of interest at radial station .865R is presented in Figure 13. Again this presents a very complex picture of the airflow at this point. The level flight point show a fairly broad vortex flowing from the leading edge that passes over all six pressure transducers at the beginning of the second quadrant. A small retreating side vortex is also visible. Also seen is the pressure increase in the second quadrant as a shock passes over the transducers. As the roll rate increases the area of supercritical flows increase, the shock becomes stronger and covers a larger area, and the retreating side vortex becomes stronger. The advancing side vortex becomes sharper and two distinct vortexes appear in cycle 30. At the end of the fourth quadrant it appears that a strong shock passes over the 0.03c tranducer and then returns only to be established once more at the start of the first quadrant.

The most significant effect of this maneuver on structural loads is seen on the pitch link loads in Figure 14. The vibratory load doubles at the peak roll rate in cycle 30 with maximum positive and negative loading occurring approximately at 90 and 180 degree respectively. The load is attributed to the increased positive loading of the first quadrant and the sharp negative loading of the second quadrant. It is interesting in this regard that the loading behavior is very similar to that seen in level flight. This suggest that a correct prediction of the control loads in level flight (the positive moment in the first quadrant and the negative load in the second quadrant) will go a long way towards the prediction of the control loads in this maneuver. In this sense the level flight case is an analog of this maneuver condition.

Pull-up Maneuver

A pull-up maneuver with a target of 2.0g at 80 KIAS was recorded on Flight 89 as Counter 27 and 16 seconds of data were obtained during the maneuver. The piloting method used to obtain the pull-up maneuver was essentially the reverse order of that used in the pushover described above. Figure 15 presents six measurements that can be used to help define the maneuver; rotor speed, airspeed, load factor, longitudinal stick, pitch attitude and rate. As can be seen, the parabolic trajectory results in 0.45g being held from the 15th to the 25th cycle, with a rapid increase to 2g which are held from the 36th to 43th cycle. The trim during the 2g is moderately steady. The rotor speed during the sustained load factor decreases from 101.8% to 101.5%. Airspeed decreases from 103 to 96 KIAS, while pitch attitude varies from 0 to 18 degrees, and pitch rate oscillates from a high of 20 degrees/second down to half that value as shown from the derivative of pitch attitude measurement (dash line)

The integrated nondimensionalized normal force and pitching moments coefficients for three radial stations (0.99R, 0.865R, 0.55R) are shown in Figure 16. Each curve presents every second revolution from the first available rotor cycle until 12 seconds into the test point, where recovery has begun. The plots of normal force at all three radial stations exhibit the classical signs of vortex loading early in the maneuver on both the advancing and retreating sides of the rotor disk. As the vertical loading reduces to 0.5g the normal force curves flatten out considerably. The vortex loading on the retreating side of the rotor, which is so prominent in the first several rotor cycles at 0.99R and 0.865R disappears completely as 0.5g is obtained. Upon

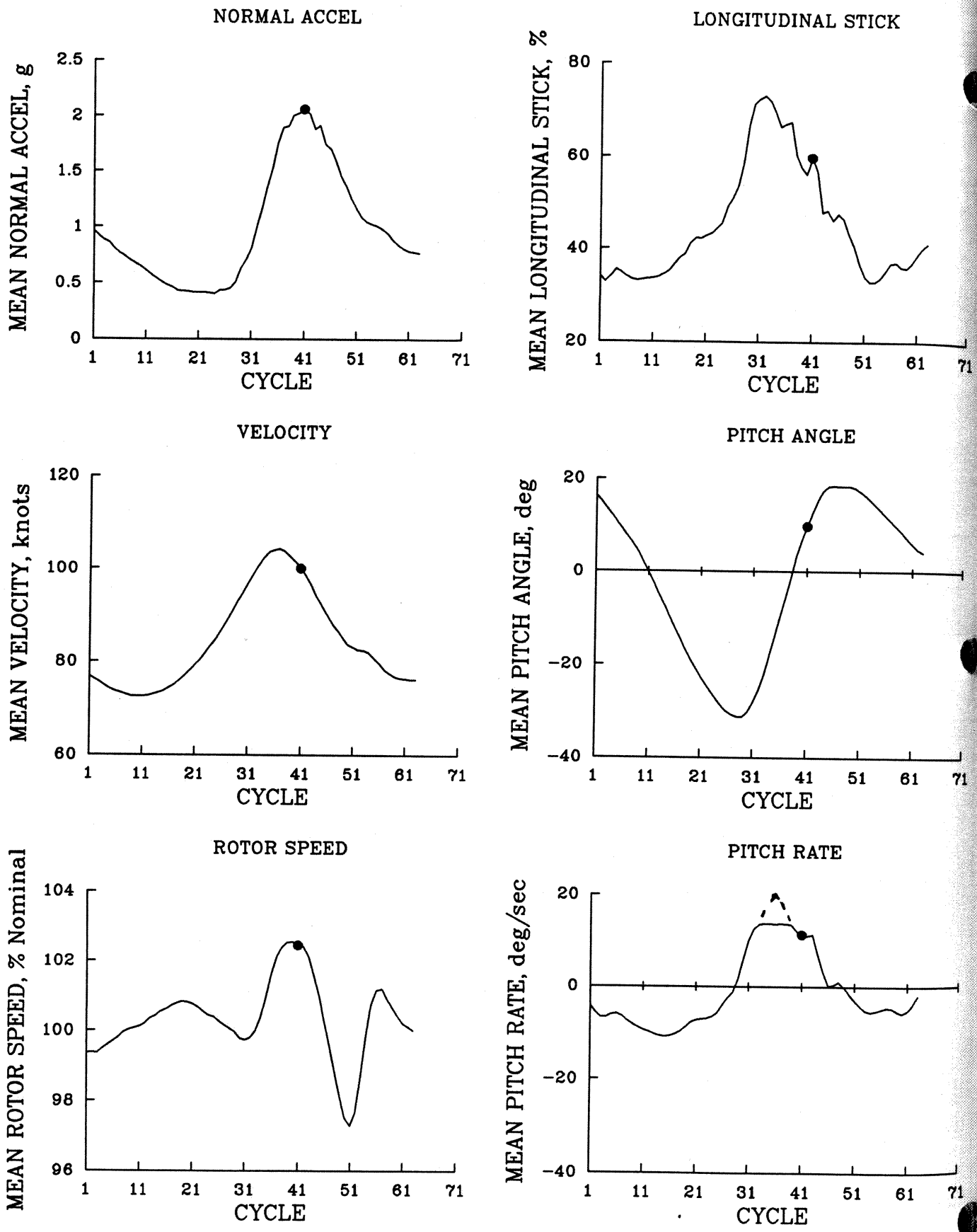

Fig. 15 Mean load factor, velocity, rotor speed, pitch rate, pitch angle, and longitudinal stick position during the poll-up maneuver (8927).

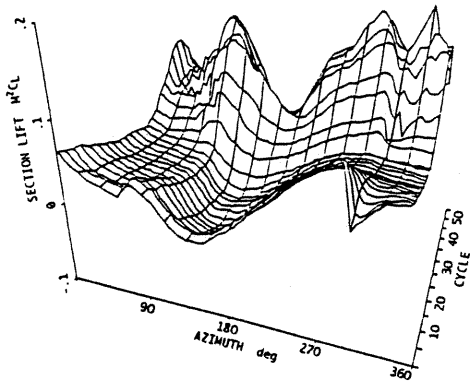

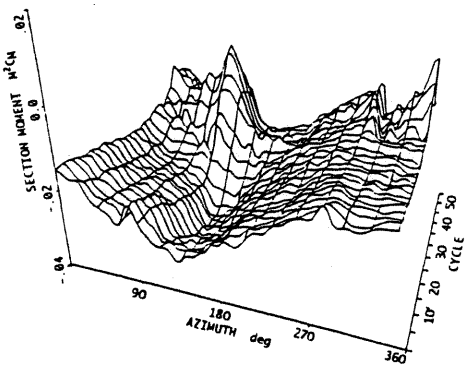

a. r/R = 0.99

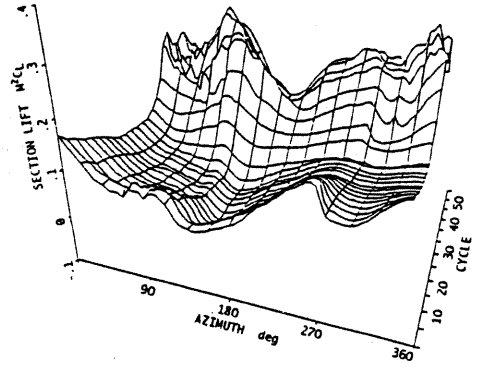

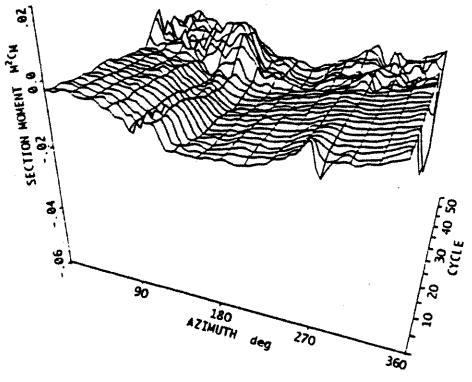

b. r/R = 0.865

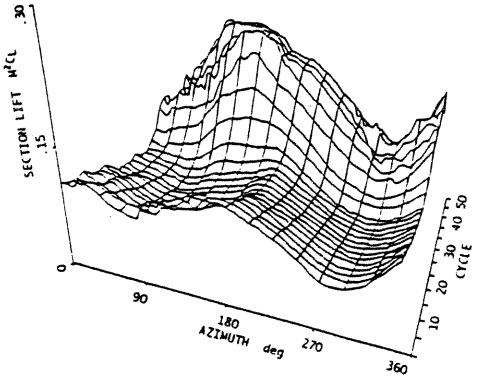

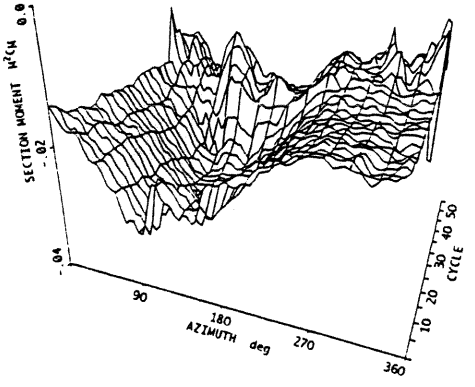

c. r/R = 0.55

Fig. 16 Section lift and pitch moment at r/R = 0.99, 0.865, 0.55 as a function of azimuth and cycle count during pull-up maneuver (8927); 0 to 60 harmonic.

increasing the vertical loading, the signs of blade vortex interaction (BVI) quickly return, however with an entirely different character than was present at the early portion of the maneuver. Instead of a single major vortex being encountered, now there are multiple vortices. The rotor is flying through its own wake, with all the interactions occurring in the first and forth quadrants. The BVI encounters extend inboard on the blade past 0.55R. This multiple vortex loading will be investigated in more detail later on in this paper.

The pitching moment coefficient meanwhile, contains much harmonic content. Again, at the beginning of the maneuver, the signs of vortex loading are present on both the advancing and retreating side at 0.99R and 0.865R and only the advancing side at 0.55R. As the load factor decreases, during the pushover, the moments generally smooth out, only to return sharply as the vertical load factor increases to 2g. Here the effects of the multiple vortex encounters manifest themselves as rapid fluctuations in moment. The first quadrant contains a rise in moment toward zero, followed by rapid decreasing moments as the blade enters the second quadrant. Throughout the second quadrant, the moments remain relatively quiescent, regaining the rise toward zero in the third quadrant, with the fluctuations of the vortex interactions returning in the forth quadrant.

The response of blade flapping and feathering is shown in Figure 17 for the pull-up maneuver. Blade flapping begins with the classical shape. The magnitude rapidly decreases as the load factor decreases, until the curve is very nearly flat. As the load factor is increased, there is a 180 degree phase shift from the initial flapping curve as the blade flaps up over the nose. As the flight path steadies and the maximum vertical loading is approached, the flapping curve returns to its classic down over the nose shape within 4 cycles. The nature of how the flapping returns to the nominal wave shape is event is hidden in this surface plot. The blade flapping during the cycle of maximum vertical loading has not yet reached the positive peak displacement observed in the surface plot. Indeed, it has a 2/rev wave shape with maximums of 6.4 degrees and 5.4 degrees at 20 and 180 degrees azimuth respectively, and its minimums of 4.4 and 4.6 degrees at 100 and 250 degrees azimuth respectively.

Blade feathering for the pull-up maneuver shows much less dynamic variation then does the flapping. Its sine wave decreases in magnitude as the maneuver is performed. As the vertical loading begins to increase from 0.5g, the feathering trace reaches its minimum amplitude. It immediately increases its feathering reaching a larger magnitude than obtained initially. As the maneuver continues into its recovery, the blade feathering reduces in magnitude.

The normal force for the cycle of maximum sustained vertical loading(cycle 41) and a cycle averaged for a level trim test point at 1.0g, and nearly the same advance ratio are compared in Figure 18. The figure presents the blade radial distribution for a single revolution.

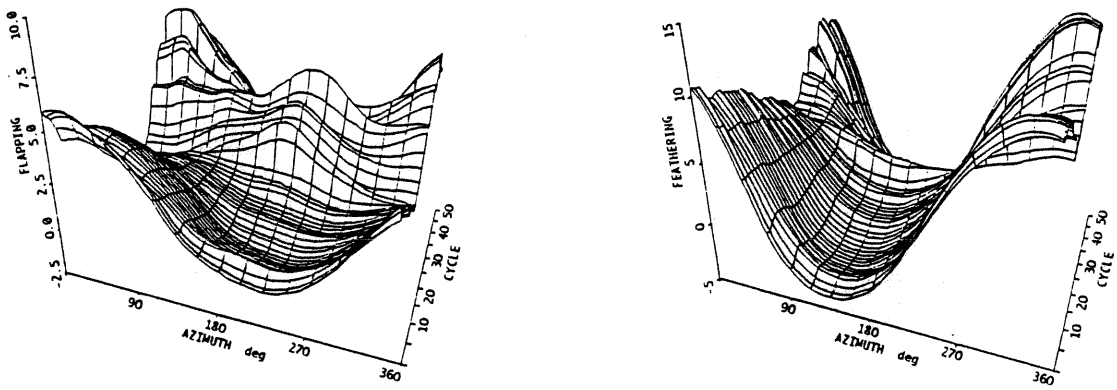

Fig. 17 Blade flapping and feathering as a function of azimuth and cycle count during pull-up maneuver (8927).

$\mu = 0.238$, $n_z * C_T/\sigma = 0.138$ (Cyc 41)
SECTION LIFT

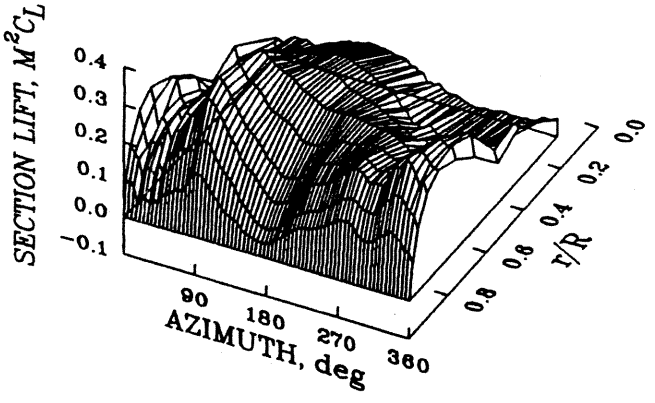

$\mu = 0.232$, $n_z * C_T/\sigma = 0.079$ (steady)
SECTION LIFT

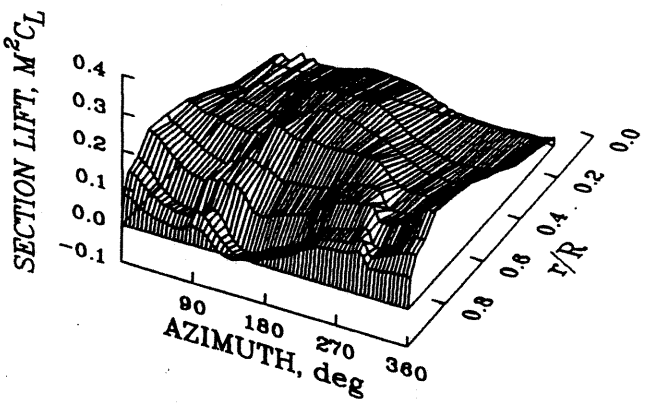

Fig 18 Comparison of section lift as a function of azimuth and radial station for cycle 41 of the pull-up maneuver (8927) and an equivalent level flight case; 0 to 60 harmonics.

The normal force curves show that at 2g there is much more unsteadiness in the first and forth quadrants than in level flight. The tip region appears to be carrying a larger percentage of the blade load on the advancing side at 2g then it does in level flight. The BVI that exists in level flight on the retreating side has vanished at the peak g loading having been replaced by multiple intersections about 20 degrees later.

In Figure 16, at 0.99R, as the vertical loading is rapidly increasing, a BVI encounter is prominent on the retreating side. This event is presented in more detail for the 0.965R in Figure 19. Here, the integrated normal force coefficients for cycles 32, 34, 36, 38 and 40 are presented. It can be seen that for cycle 32, there is a loading peak at $\psi = 90$ degrees, and a BVI event at $\psi = 280$ degree. Just 2 revs later, on the retreating side, a second large BVI event manifests itself at $\psi = 300$ degrees, with another of less magnitude appearing at $\psi = 330$ degrees. The sharp definition of the event at $\psi = 300$ degrees leads to the conclusion that the vortex has been intersected very nearly through the center of the vortex core. On the advancing side of the rotor a modest BVI has appeared at $\psi = 70$ degrees. It should be pointed out here, that the vertical spacing of the curves in this figure are the result of the increasing rotor loading and not an artificial spreading of the data as is often done for clarity sake. By cycle 36, the large event at $\psi = 280$ degrees has reduced in magnitude and its features have been quite rounded. The BVI that appeared two cycles earlier at $\psi = 300$ degrees has lost much of its intensity, but other interactions have appeared from $\psi = 340$ degrees to 10 degrees. On the advancing side where there had been a single BVI during cycle 34, there are now 4 between $\psi = 50$ and 80 degrees. When cycle 38 occurs, four new interactions have appeared in the area from $\psi = 320$ to340 degrees, and there are now 15 interactions over the 120 degree arch from $\psi = 320$ to 90. The interactions that remain from cycle 36 have lost

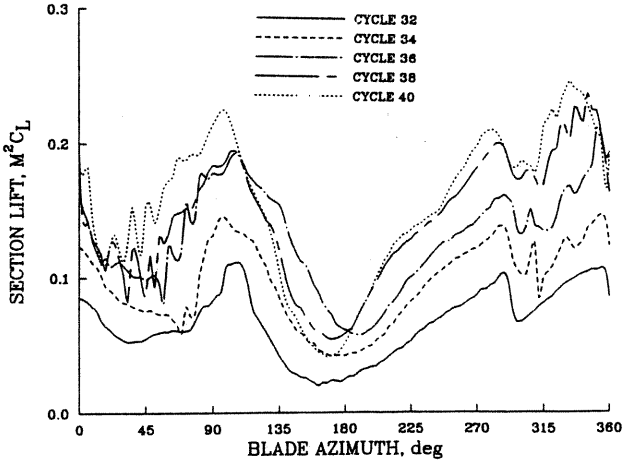

Fig. 19 Section lift at 0.965R for cycles 32-40 of the pull-up maneuver (8927); 0 to 60 harmonics

intensity, while the new ones that appear are quite large. As the maneuver continues on the cycle 40, which is essentially at the 2g condition, and is the cycle proceeding that shown in Figure 18, no new interactions occur although there is some shifting of the azimuthal locations of those that do appear.

Finally, the blade structural loads for the 2g condition and level trim are compared. Figure 20 presents the following: blade torsion at 0.30R, blade edgewise at 0.113R and 0.60R, and flap wise bending moments at 0.60R, pitch link load, and main rotor torque. With the exception of the pitch link load curve, the steady loading have been removed from the plots. In some instances this is due to large shifts in the measurements due to the maneuver (i.e. rotor torque), and in others cases, the strain gages drifted during the test with the result that the steady terms are not reliable.

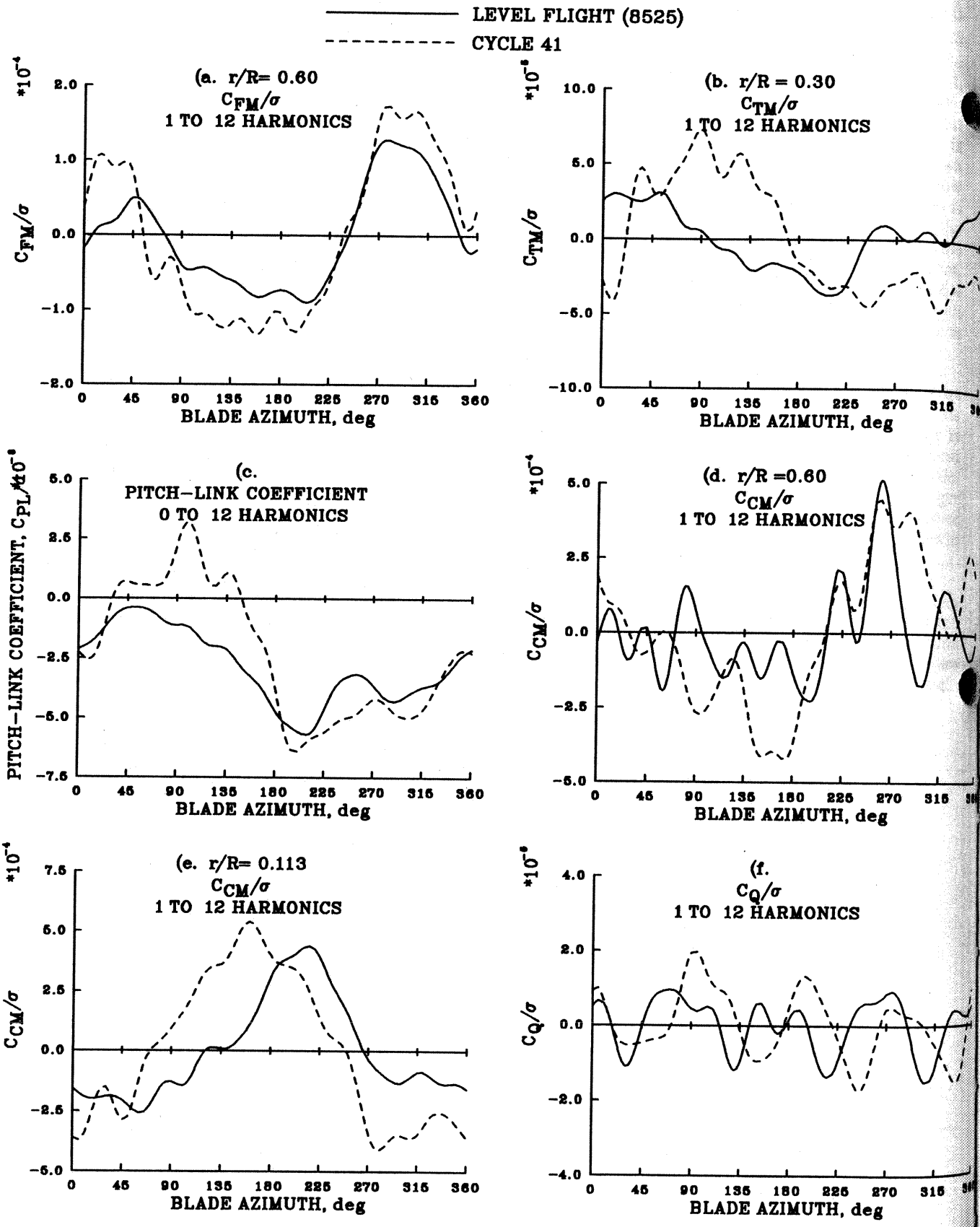

Fig. 20 Comparison of blade flap bending at 0.60R (a., blade torsional moment at 0.30R (b., pitch link load (c., edge bending at 0.113R (d. and 0.60R (e., and main rotor torque (f. for cycle 41 of the pull-up maneuver (8927) and an equivalent level flight case; 1 to 12 harmonics.

Flapping Moment coefficient at 0.60R, , figure 20a, shows large amplitudes at 11/rev (46 Hz) for the 2g condition where the trim condition does not. This is a response at the blade's fourth natural flapping frequency. Refs. 4 & 5 independently reported a measured blade frequency of 42 hertz for flapping in a non-rotating condition. It can be expected that the centrifugal loading of rotation will effectively increase the stiffness of the system, resulting in an modest increase in the natural frequencies. Comparing the two curves, it can be seen that level flight peak to peak is .00022 versus .00034 for the pull-up, and that there is band edge at $\psi = 280$ degrees. There is no phase shift between these two test conditions. It is noted that the phase behavior does not change significantly between the two conditions.

For the blade torsion measurement at 0.30R, figure 20b, as with the normal force, the pull-up results in a significant increase in frequency content as well as increase in peak to peak magnitude. The signal for the pull-up shows several interesting characteristics; a prominent 6 per rev, a less prominent 11 per rev, and a striking change in sign just as the blade passes over the tail. Here the blade goes from a nose down pitching moment to nose up with essentially the same magnitude. The 11 per rev is the excitation of the 2nd torsion natural frequency, which was measured at 44.5 Hz from Ref. 4.

The pitch link, figure 20c, shows that at the 2g, condition, the first two quadrants are now positively loaded with a rapid plunge to its largest negative value at $\psi = 200$ degrees. In level flight however, the link load smoothly transitions from it's maximum to minimum link load over the first two quadrants. The frequency content of the pitch links during the pull-up maneuver is greater in magnitude then that contained in the level trim condition

The edgewise bending curve at 0.60R, figure 20d, shows a that again the basic wave shape is unchanged. There is a delay of 20 degrees in the rise on the retreating side. The harmonic content is essentially unchanged, although there is considerable increase in magnitude. The plot of blade root edgewise bending, figure 20e, shows the 1st harmonic is prominent with a 30 degree phase shift difference between level flight and 2g

The plot of main rotor torque, figure 20f, shows the prominent four per rev character of rotor torque. The steady torque values for these two conditions were significantly different, with the value at this cycle in the pull-up maneuver having dropped to one tenth the value at trim. Each of the four peaks in level trim are quite wide, and seem to be the result of two signals superimposed. The curve for the pull-up seems to be just a single 4-per-rev signal with a much smaller second frequency of 8 per-rev also present.

Concluding Remarks

The effects of maneuvering flight on rotor load distribution, aerodynamics and structural loading have been qualitatively examined. The maneuvers covered here offers only a tantalizing glimpse into the aerodynamic complexities of non-steady maneuvering flight. As would be expected the integrated Airloads rise as the rotor is load factor increases. The detailed aerodynamic loading appears to be more complex than in level flight. This is particularly true in the character??? variety of vortex loading. However, it also appears that the general behavior exhibited under high load factor conditions is very similar to level flight conditions and, therefore, level flight or wind tunnel data represent an analog for maneuver flight and a first tool of analysis.

References

1. Kufeld, R. and Loschke, P., "UH-60 Airloads Program: Status and Plans," AIAA Aircraft Design, Systems, and Operations Meeting, September 1991.

2. McHugh, Frank J., "What Are the Lift and Propulsive Force Limits at High Speed for the Conventional Rotor?," American Helicopter Society 34th Annual Forum, May 1978, pp. 1-12.

3. Maier, Thomas H., and Bousman, William G., "An Examination of the Aerodynamic Moment on Rotor Blade Tips Using Flight Test Data and Analysis," Eighteenth European Rotorcraft Forum, September 1992.

4. Kufeld, R. and Nguyen, D., "Full-Scale UH-60A Rotor Blade Nonrotating Modal Analysis Shake Test", NASA TM 101005, Nov 1989.

5. Hamade, D. and Kufeld, R., "Modal Analysis of UH-60A Instrumented Rotor Blades", NASA TM 4239, Nov 1990.